

Fusion Peptide of Influenza Hemagglutinin Requires a Fixed Angle Boomerang Structure for Activity*

Received for publication, November 15, 2005, and in revised form, December 22, 2005. Published, JBC Papers in Press, December 28, 2005, DOI 10.1074/jbc.M512280200

Alex L. Lai[‡], Heather Park[§], Judith M. White[§], and Lukas K. Tamm^{†1}

From the Departments of [‡]Molecular Physiology and Biological Physics and [§]Cell Biology, University of Virginia, Charlottesville, Virginia 22908

The fusion peptide of influenza hemagglutinin is crucial for cell entry of this virus. Previous studies showed that this peptide adopts a boomerang-shaped structure in lipid model membranes at the pH of membrane fusion. To examine the role of the boomerang in fusion, we changed several residues proposed to stabilize the kink in this structure and measured fusion. Among these, mutants E11A and W14A expressed hemagglutinins with hemifusion and no fusion activities, and F9A and N12A had no effect on fusion, respectively. Binding enthalpies and free energies of mutant peptides to model membranes and their ability to perturb lipid bilayer structures correlated well with the fusion activities of the parent full-length molecules. The structure of W14A determined by NMR and site-directed spin labeling features a flexible kink that points out of the membrane, in sharp contrast to the more ordered boomerang of the wild-type, which points into the membrane. A specific fixed angle boomerang structure is thus required to support membrane fusion.

Enveloped viruses enter cells by membrane fusion. Some viruses fuse with the plasma membrane at the cell surface, but others are first taken up by receptor-mediated endocytosis and subsequently fuse with the endosomal membrane triggered by the acidic pH that prevails in the endosome. Influenza virus belongs to the second group. The major glycoprotein on the viral surface, influenza hemagglutinin (HA),² binds to sialic acid residues on the surface of host cells and undergoes a dramatic conformational change when the pH drops below ~5.3 in the endosome (1–3). This conformational change, among other rearrangements, exposes an N-terminal quite hydrophobic peptide of HA2, the smaller of the two HA subunits, and makes it available for interaction with the lipid bilayer of the endosomal membrane. Because this peptide is essential for fusion and thus very highly conserved in sequence among all known strains of influenza virus, it has been termed the “fusion peptide.” Because influenza HAs are trimers consisting of three HA1 and three HA2 subunits and because several HA molecules are needed

to build a single fusion site, it is likely that multiples of three fusion peptides insert into the target membrane to initiate fusion between the viral and the target membrane. The C-terminal end of the HA2 chain contains the transmembrane domain that anchors HA in the viral membrane. A salient feature of the pH-induced conformational change of HA is that the ectodomain between the fusion peptide and the transmembrane domain rearranges such that the N and C termini end up at one end of the rod-shaped molecule in very close proximity to each other (4) and thus potentially allow for a mutual contact between the fusion peptides and the transmembrane domains at some point during the fusion reaction. An assessment of the structures of the fusion peptides and transmembrane domains before, during, and after fusion is therefore of high interest in our quest to understand the mechanism of influenza HA-mediated membrane fusion at the molecular level.

We have recently determined the structure of the wild-type fusion peptide of HA in dodecylphosphocholine (DPC) micelles by NMR and in lipid bilayer model membranes by EPR spectroscopy (5). The ~24-residue fusion peptide features two short helices at pH 5 which are separated by a ~105° kink at Asn-12. The N-terminal helix is more hydrophobic and contains a conserved glycine edge followed by Glu-11 on one face. The C-terminal half is more amphipathic with a number of polar and charged residues on its upper face and bulky hydrophobic residues including Trp-14 on its lower membrane-dipped face. This structure together with the close proximity of the N and C termini in the low pH crystal structure of the ectodomain and the lower energy of the pH 5 compared with the pH 7 conformation have led to the formulation of the spring-loaded boomerang model of influenza HA-mediated membrane fusion (6). The angled boomerang structure may be required for membrane fusion. For example, the fusion peptide mutant G1V, which in the context of full-length HA is completely defective in mediating membrane fusion (7), exhibits a linear helical structure in lipid model membranes (8). To test whether a boomerang structure is necessary and sufficient for membrane fusion, we targeted the residues that define the angle of the boomerang by site-directed mutagenesis. We analyzed the mutants both in full-length HA to assess their fusion activity in red blood cell (RBC)-cell fusion assays, and in peptide models to assess their structures and lipid interactions in model membranes. Our structure-energetics-function correlations support the notion that a specific fixed angle boomerang is required for tight interactions with lipids of the target membrane and for membrane fusion.

EXPERIMENTAL PROCEDURES

Mutagenesis—Mutations were introduced into the pTM1-HA vector with the QuikChange site-directed mutagenesis kit (Stratagene). Primers were purchased from IDT DNA, Inc. The E11A and W14A mutant HAs were sequenced completely. For the other mutants, the sequence around the fusion peptide region (> 500 bp) was checked.

HA Expression—Subconfluent monolayers of CV-1 cells in 6-cm dishes were infected with modified *Vaccinia ankara*, which encodes T7

* This work was supported by National Institutes of Health Grants R37 AI30557 (to L. K. T.) and R01 AI22470 (to J. M. W.). The costs of publication of this article were defrayed in part by the payment of page charges. This article must therefore be hereby marked “advertisement” in accordance with 18 U.S.C. Section 1734 solely to indicate this fact. The atomic coordinates and structure factors (code 2DCI) have been deposited in the Protein Data Bank, Research Collaboratory for Structural Bioinformatics, Rutgers University, New Brunswick, NJ (<http://www.rcsb.org/>).

¹ To whom correspondence should be addressed: Dept. of Molecular Physiology and Biological Physics, University of Virginia Health System, P. O. Box 800736, Charlottesville, VA 22908. Tel.: 434-982-3578; Fax: 434-982-1616; E-mail: lkt2e@virginia.edu.

² The abbreviations used are: HA, hemagglutinin; ATR, attenuated total reflection; DPC, dodecylphosphocholine; FACS, fluorescence-activated cell sorter; FTIR, Fourier transform infrared; MES, 4-morpholineethanesulfonic acid; NOESY, nuclear Overhauser effect spectroscopy; RBC, red blood cell; TOCSY, total correlation spectroscopy; POPC, 1-palmitoyl-2-oleoyl-*sn*-glycero-3-phosphocholine; POPG, 1-palmitoyl-2-oleoyl-*sn*-glycero-3-phosphoglycerol; SUV, small unilamellar vesicle; NIEDDA, nickel (II)-ethylendiamine-*N,N'*-diacetic acid.

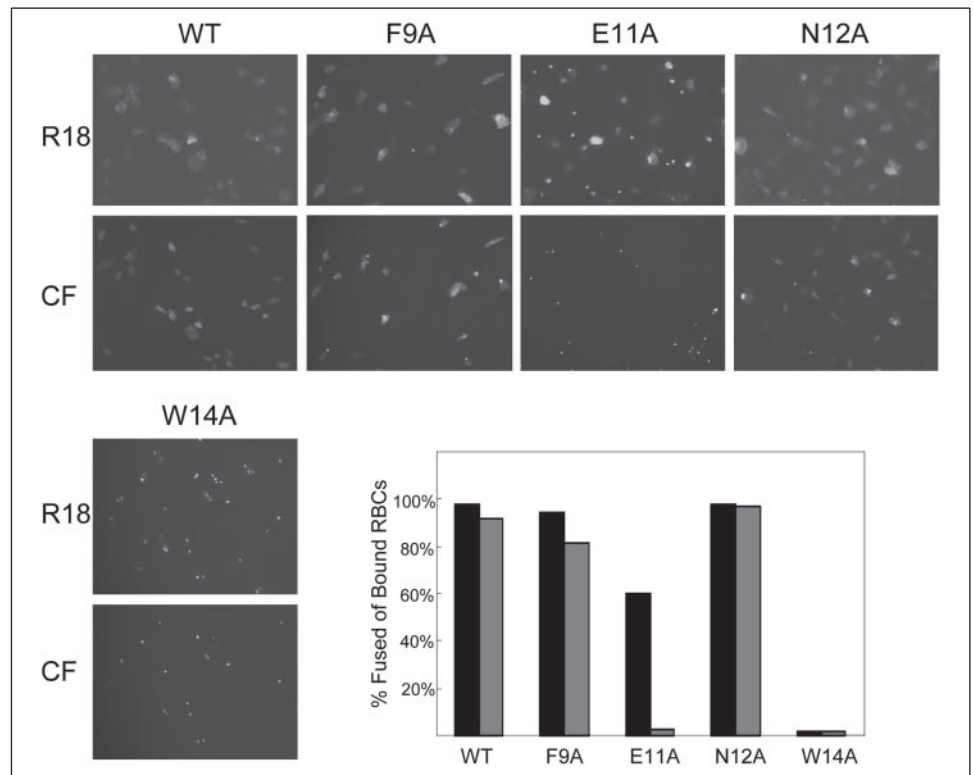


FIGURE 1. Fusion activity of HAs with mutations in the fusion peptide kink region. R18 and CF double-labeled RBCs were bound to CV-1 cells that had been transfected with DNA encoding wild-type (WT) or mutant HA and treated with neuraminidase, trypsin, and fetal bovine serum. The micrographs show cells after triggering fusion with pH 5 fusion buffer and examination for lipid mixing (R18) and contents mixing (CF) under a fluorescence microscope. A quantification of hundreds of fusion events such as those shown in the micrographs and expressed as the percentage of cells with bound RBCs that undergo fusion with CV-1 cells is shown in the panel on the bottom right.

polymerase, for 1 h at 37 °C with rocking every 15 min. The cells were then washed twice with Dulbecco's phosphate-buffered saline, transfected with 1 μ g of wild-type or mutant pTM1-HA DNA using 12 μ l of Mirus Transit (Panvera), and incubated in Opti-MEM I at 37 °C for 5 h. Finally, the DNA/Transit mixture was replaced with Iscove's modified Dulbecco's medium supplemented with 10% fetal bovine serum, 1% glutamine, and 1% penicillin/streptomycin, and the cells were cultured for a further 16 h.

Red Blood Cell Fusion Assay—Fresh human RBCs were double labeled with R18 and CF (Molecular Probes, Inc.), and fusion assays with HA-expressing cells were performed under a fluorescence microscope (Zeiss) as described previously (9). RBC binding and lipid and contents mixing events were counted. Fusion was expressed as lipid mixing ratio (CV-1 cells that were stained with R18 divided by CV-1 cells that bound RBCs) and contents mixing ratio (CV-1 cells that were stained with CF divided by CV-1 cells that bound RBCs).

Red Blood Cell Dequenching Assay—HA-expressing CV-1 cell, R18-labeled RBC complexes were prepared, and fusion was measured by dequenching in a spectrofluorometer (SPEX Fluorolog) at 37 °C as described previously (9). The percent fluorescence dequenching (FDQ) was calculated as

$$\text{FDQ} = (F_1 - F_0 / F_{\text{det}} - F_0) \times 100 \quad (\text{Eq. 1})$$

where F_0 is the fluorescence during the initial pH 7.0 incubation, F_1 is the fluorescence at the end of the pH 5 incubation period and before the addition of detergent, and F_{det} is the fluorescence in the presence of detergent. The initial rates of fusion were determined from the slope of the initial increase of the fluorescence dequenching signal.

Immunoprecipitation and Fluorescence-activated Cell Sorter (FACS)—Biotinylation, immunoprecipitation, and Western blot analysis of cell surface proteins were conducted as described previously (9). Cell surface expression of HA was measured in a FACS (BD Biosciences) as described previously (7).

Peptides and Lipids—All peptides were synthesized by solid phase synthesis by the Biomolecular Research Facility at the University of Virginia. All lipids were purchased from Avanti Polar Lipids (Alabaster, AL).

Small Unilamellar Lipid Vesicles—Desired amounts of POPG and POPC from chloroform stock solutions were dried at the bottom of glass test tubes overnight under vacuum. pH 5 buffer (5 mM HEPES, 10 mM MES, pH 5) was added, and the suspension was vortexed to give a 5 mM lipid dispersion. The dispersion was then sonicated in an ice-water bath using a titanium tip ultrasonicator (Branson) for ~1 h at 50% duty cycle until the solution was transparent.

Isothermal Titration Calorimetry—All measurements were carried out at 25 °C in a high sensitivity MCS titration calorimeter (MicroCal, Inc.) as described previously (10). To measure reaction enthalpies, 10- μ l aliquots of 20 μ M peptide were injected into the sample cell containing 2 ml of 5 mM POPC:POPG (4:1) SUVs. To measure free energies, 10- μ l aliquots of 5 mM POPC:POPG (4:1) SUVs were injected into the sample cell containing 2 ml of 20 μ M peptide. Enthalpies of dilution and mixing were determined by running control experiments with the polar C-terminal host peptide.

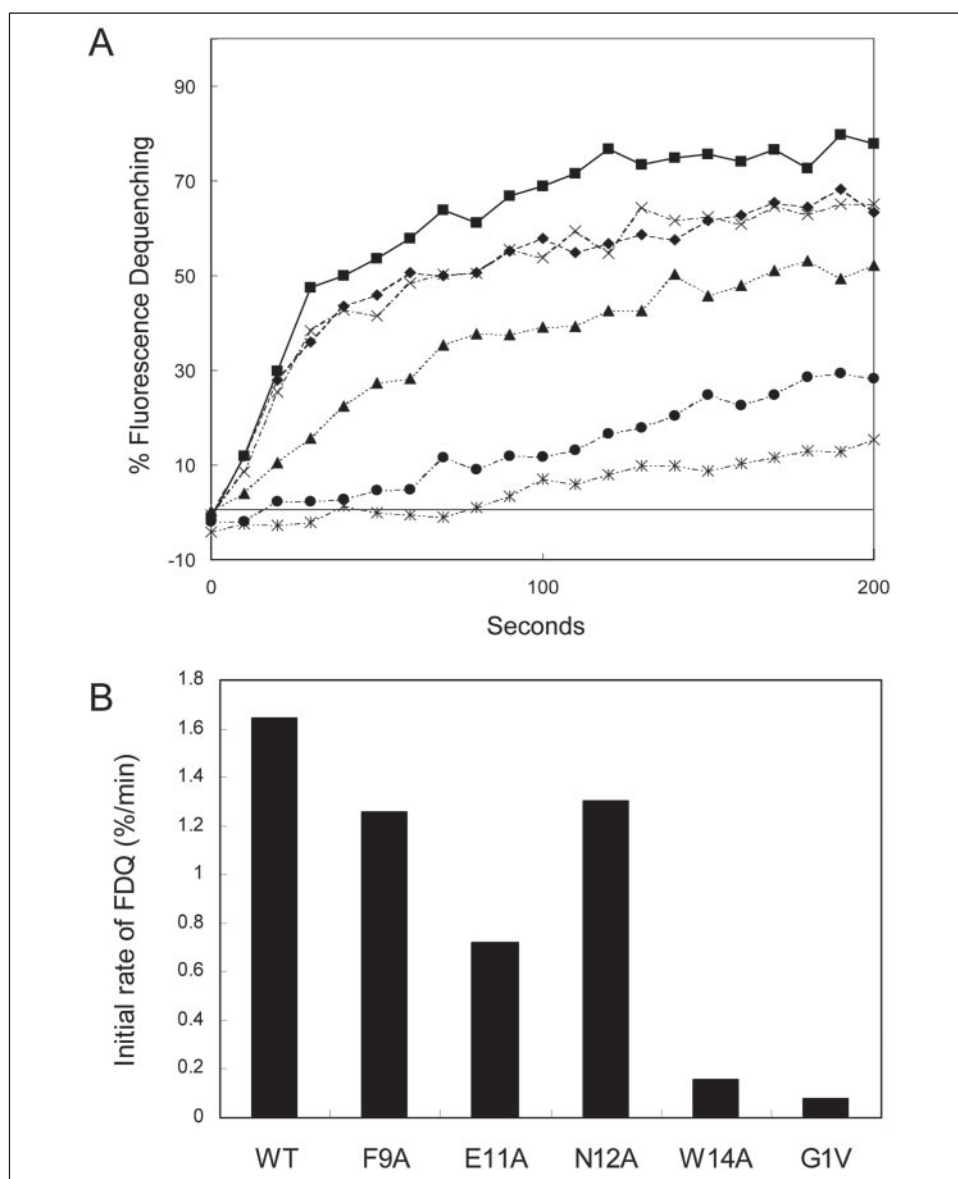
Analysis of Binding Data—Intrinsic partition coefficients, K_0 , were calculated from the apparent partition coefficients, K_{app} , using the Gouy-Chapman theory with a membrane surface potential ψ_0 of -96.1 mV and Equation 2,

$$K_0 = K_{\text{app}} \exp(z_p F \psi_0 / RT) \quad (\text{Eq. 2})$$

where z_p = peptide charge, F = Faraday's constant, R = gas constant, and T = absolute temperature.³ Free energy changes associated with the

³ The nominal charges of the wild-type, F9A, N12A, and W14A peptides are +1.0, and this charge has been used for z_p in these calculations. An effective charge of +1.22 was used for the E11A peptide, which is less than its nominal charge of +2.0. The effective charge of E11A was estimated based on an expected pK_a shift of +0.55 of a glutamate at a negatively charged surface at pH 5.

FIGURE 2. Fluorescence dequenching of the lipid probe R18 upon fusion of labeled RBCs with HA-expressing CV-1 cells measured by spectrofluorometry. A, kinetics of fluorescence dequenching. ■, wild-type (WT); ◆, F9A; ×, N12A; ▲, E11A; ●, W14A; *, G1V. B, initial rates of fusion after acidification to pH 5.



binding of the fusion peptides to lipid bilayers were calculated using the following equation.⁴

$$\Delta G = -RT \ln(55.5K_0) \quad (\text{Eq. 3})$$

Entropy changes were calculated by Equation 4.

$$\Delta G = \Delta H - T\Delta S \quad (\text{Eq. 4})$$

Circular Dichroism and Fourier Transform Infrared Spectroscopy—0.1 mg/ml peptide was added to SUVs composed of POPC:POPG (4:1) or DPC micelles at a ratio of 1:200 peptide:lipid and degassed for 5 min at room temperature before measurement. CD spectra were collected at 25 °C on an AVIV model 215 spectropolarimeter. The signals from pure SUVs or DPC micelles were subtracted from the sample spectra as blanks. For FTIR, planar phospholipid bilayers supported on germanium ATR plates were prepared as described previously (11). The substrate-supported monolayer was 1,2-dimyristoyl-*sn*-glycero-3-phosphocholine, and the monolayer exposed to the buffer

compartment was POPC:POPG (4:1). Desired amounts of peptide in pH 5 buffer were added to the sample cell, incubated for 5 min at room temperature, and excess unbound peptide was washed away with pH 5 buffer made in D₂O. Polarized spectra were recorded on a Bruker Optics Vector 22 FTIR spectrometer. Order parameters and average insertion angles were calculated as described previously (12).

NMR Spectroscopy and Structure Calculation—NMR spectra were collected on a Varian Inova 600 MHz spectrometer, processed, and structures were calculated as described previously (8). The 100 conformers with the lowest energy target function values were energy-minimized using the program OPAL with the Amber94 force field (13). The energy-minimized conformers were aligned and displayed using the program MOLMOL (14).

EPR Spectroscopy and Docking of NMR Structures to EPR Depth Data—Peptides containing single cysteines were labeled with the methanethiosulfonate spin label and purified as described previously (8). Power-saturation EPR measurements of spin-labeled peptides bound to lipid vesicles in the presence of N₂, air, and N₂ with 20 mM NiEDDA were performed with a Varian E-line Centuries Series spectrometer as described previously (8). Representative NMR conformers with substi-

⁴ The value of 55.5 M accounts for the cratic contribution of the molarity of water.

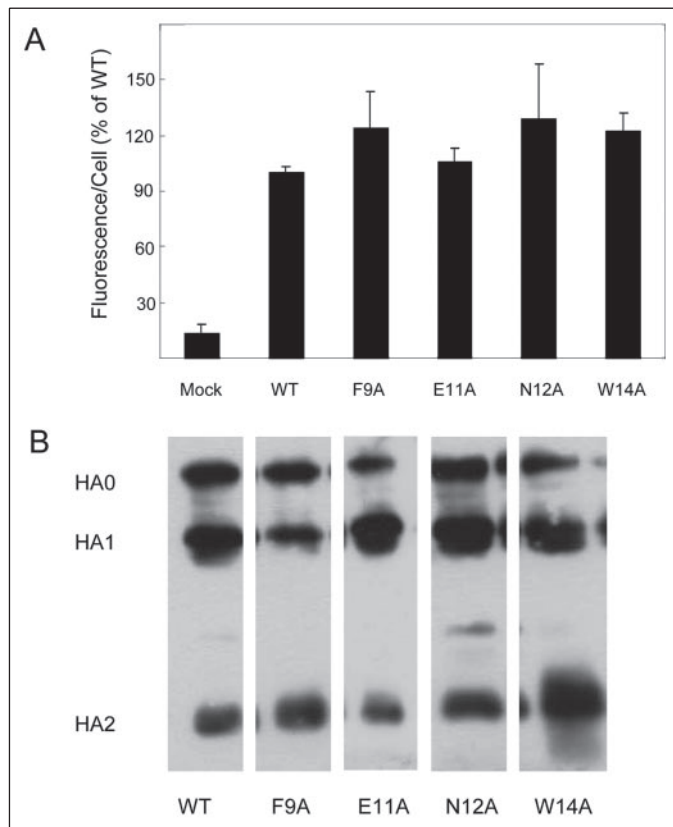


FIGURE 3. Expression and processing of wild-type (WT) and mutant HAs on the surface of CV-1 cells. *A*, FACS analysis of fluorescence intensity/cell expressed as a percent of wild-type. *B*, SDS-polyacrylamide gels of immunoprecipitated HA demonstrating cleavage of HA0 into HA1 and HA2 after treatment with trypsin.

tuted spin labels were docked to lipid bilayers with the program Insight II (Accelrys). The dihedral angles χ_1 and χ_2 of the spin label were set to 300° (15), and the values of χ_3 , which can assume values of $+90^\circ$ (*p*) or -90° (*n*), were determined for each site by energy minimization with the Amber force field. The energy-minimized structure had the χ_3 combination *nnnp* for the four consecutively labeled residues.

RESULTS AND DISCUSSION

Fusion Activity of HA Mutants—The angle of the boomerang of the fusion peptide structure in membranes is stabilized by hydrogen bonds and hydrophobic interactions between bulky apolar residues distributed around Asn-12, which forms the apex of the structure. To examine the importance of the kink region for fusion, we individually changed four potentially critical residues, namely, Phe-9, Glu-11, Asp-12, and Trp-14 to alanines to make mutant HAs designated F9A, E11A, N12A, and W14A, respectively. These amino acids were targeted because they each contribute hydrogen bonds to the kink in the wild-type fusion peptide (5). The aromatic side chains of Phe-9 and Trp-14, in addition, appear to contribute hydrophobic interactions to the structural definition of the kink. CV-1 cells were transfected with plasmids harboring HA with or without the respective mutations. Fusion activities of cells expressing the wild-type and mutant HAs were measured by two different methods. Fluorescence microscopy was used to observe lipid and contents mixing at the single cell level at a fixed time point, and spectrofluorometry was used to measure the initial kinetics of lipid mixing in populations of cells. In both cases, fluorescently labeled RBCs served as target cells.

For fluorescence microscopy, the RBCs were labeled with the lipid probe octadecylrhodamine B chloride (R18, red) and the contents probe

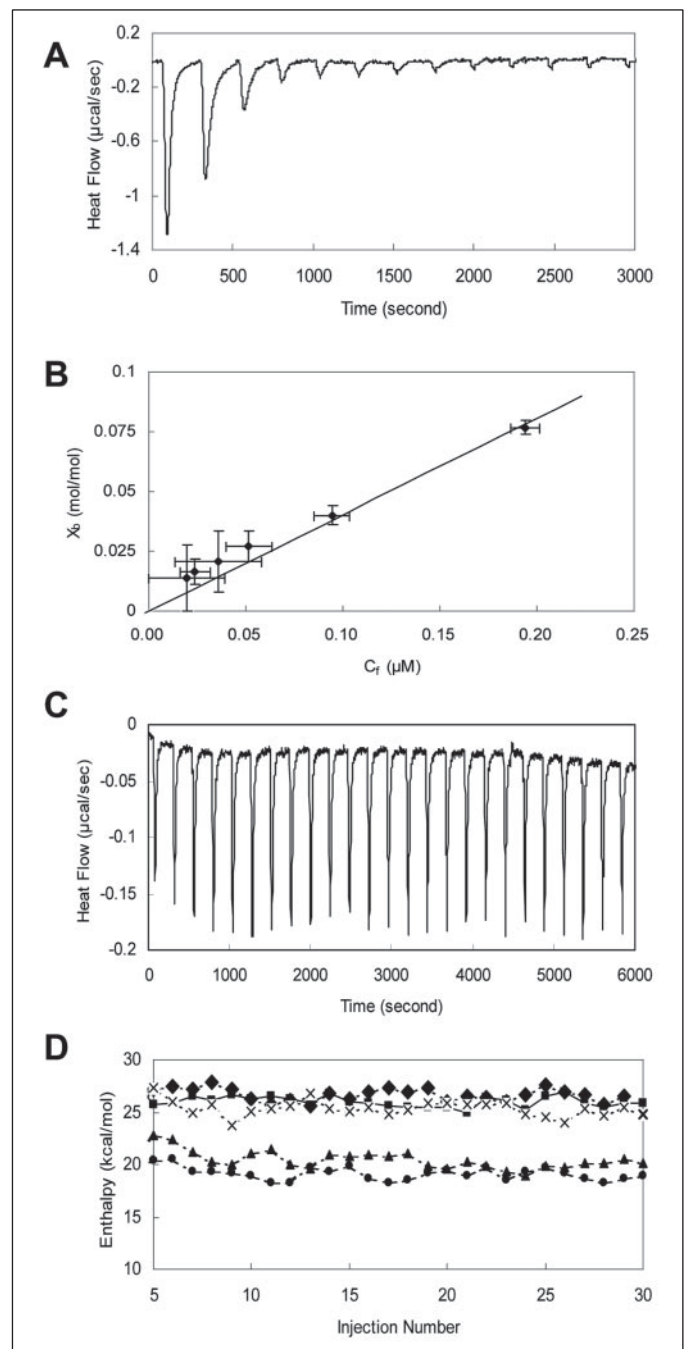


FIGURE 4. Binding of fusion peptides to lipid bilayers composed of POPC:POPG (4:1) by isothermal titration calorimetry. *A*, measurement of binding equilibrium by titration of SUVs to a fixed amount of the F9A fusion peptide. *B*, binding curve of the F9A fusion peptide, expressed as mol fraction peptide/lipid bound versus free peptide, derived from the isothermal titration calorimetry data of *A*. *C*, measurement of enthalpy change by titration of the F9A fusion peptide to a large excess of lipid. *D*, reaction enthalpies of fusion peptide binding to POPC:POPG (4:1) bilayers. ■, wild-type; ◆, F9A; ×, N12A; ▲, E11A; ●, W14A. All measurements were conducted at pH 5 and 25°C .

carboxyfluorescein (CF, green). The RBCs were first bound to HA-expressing cells that had been pretreated with a small amount of trypsin to cleave inactive HA0 into active HA1 and HA2. Fusion was induced with a 5-min pulse of pH 5 fusion buffer at 37°C , and the reneutralized samples were observed under a fluorescence microscope. Cells were classified as “fully fused” when the red and green dyes had been transferred to the CV-1 cell, as “hemifused” when only the red dye had been transferred, and as “not fused” when neither dye had been transferred.

TABLE 1

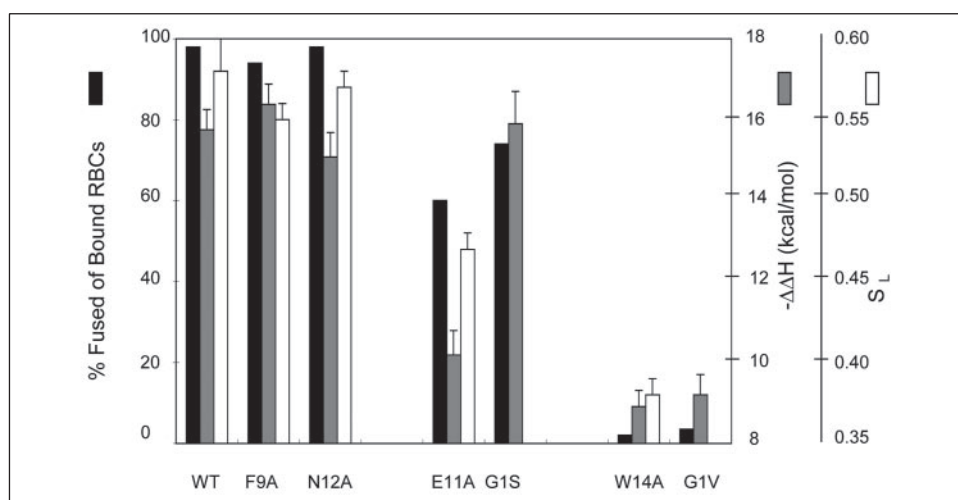
Thermodynamic parameters of fusion peptide binding to lipid bilayers composed of POPC:POPG (4:1) at pH 5

Results are averages from three independent experiments each. WT, wild-type.

Peptide	$K_{app}/10^5$ M^{-1}	$K_o/10^4$ ^a M^{-1}	$\Delta\Delta G^a$ kcal/mol	$\Delta\Delta H$ kcal/mol	$-T\Delta\Delta S$ kcal/mol
WT	6.3 ± 0.5	1.5 ± 0.1	-7.2 ± 0.4	-15.8 ± 0.5	8.6 ± 0.6
F9A	5.1 ± 0.6	1.2 ± 0.2	-7.0 ± 0.7	-16.4 ± 0.5	9.4 ± 0.9
E11A	13.3 ± 1.9	1.4 ± 0.3	-7.1 ± 0.7	-10.2 ± 0.6	3.1 ± 0.9
N12A	5.5 ± 0.6	1.3 ± 0.3	-7.1 ± 0.6	-15.1 ± 0.6	8.0 ± 0.9
W14A	0.50 ± 0.04	0.12 ± 0.01	-5.6 ± 0.3	-8.9 ± 0.4	3.3 ± 0.5

^a K_o and $\Delta\Delta G$ were calculated individually for each experiment and then averaged.

FIGURE 5. Correlation of fusion activity (lipid mixing by fluorescence microscopy), enthalpy of lipid binding, and lipid perturbation (lipid order parameter, S_l) of wild-type (WT) and mutant HAs and corresponding fusion peptides. The fusion data for G1S and G1V are from Ref. 7, and the binding data for G1S and G1V are from Ref. 10. Recall that content mixing assays, shown in Fig. 1 and Ref. 7, show high fusion for first group and practically no fusion for the latter two groups of mutants.



The results are shown in Fig. 1. The F9A and N12A mutants behaved similarly to wild-type HA: they underwent lipid and contents mixing, indicating full fusion. E11A induced lipid mixing in ~60% of all cells with bound RBCs and essentially no contents mixing. This is the hallmark of hemifusion. W14A did not show lipid or contents mixing. Although W14A is essentially blocked before reaching the hemifusion stage, 13% showed a small amount of partial lipid mixing, reminiscent of a fusion phenotype described recently (16).

Spectrofluorometric lipid mixing experiments are presented in Fig. 2. They confirm the graduated fusion activities of the different HA mutants. Wild-type, and F9A HAs exhibited similar initial rates of fusion, whereas those of E11A and particularly W14A were distinctly slower. The results obtained with W14A were also compared with the well established nonfusing HA fusion peptide mutant G1V (7). Both have very low initial rates of fusion, but the signal of W14A creeps up very slowly, which is probably a result of the spurious partial lipid mixing that we observed with this mutant in the single cell fusion assays. One might therefore call W14A "severely fusion compromised." However, because the initial rates of fusion of G1V and W14A are almost zero, and because only very limited partial fusion was ever observed with W14A in the fluorescence microscope fusion experiments, we hereafter term W14A as "nonfusogenic." In conclusion, N12A and F9A are identified as having fully fused phenotypes, E11A as having a hemifusion phenotype, and W14A as having a nonfusion phenotype.

Except for Glu-11, these residues have not been targeted before by mutagenesis. Glu-11 was replaced with a Gly by Gething *et al.* (17) and Schoch and Blumenthal (18) and with a Val by Steinhauer *et al.* (19). Although the E11G (but not the E11V) mutant was impaired in heterokaryon formation, the authors of the first two papers noted fusion of horseradish peroxidase- or fluorescent dextran-loaded RBCs. These differences may be caused by either the specific substitutions or differences in expression levels.

Expression and Processing of Mutant HAs on the Cell Surface—Experiments were conducted to ascertain that differences in surface expression and the ability of HA to be cleaved by trypsin into HA1 and HA2 were not responsible for the different fusion activities of the mutant HAs. To measure surface expression, the HA-expressing cells were labeled with an anti-HA monoclonal antibody followed by a fluorescein-conjugated secondary antibody, and their fluorescence distribution was measured with a FACS. This experiment yields information on the percentage of HA-expressing cells as well as on the relative amount of HA expressed per cell. We noted that a smaller percentage of cells expressed E11A than cells that expressed all other mutants and wild-type. However, all cells that did express E11A did so at a level comparable with the wild-type and all other mutants (Fig. 3A). Therefore, any fusion defects cannot be the result of differences in protein level on the expressing cell surface.

To determine whether surface-expressed HAs were processed properly by trypsin, transfected and trypsin-treated CV-1 cells were labeled with sulfo-NHS-LC-biotin. The cells were then lysed, and HA was immunoprecipitated with the anti-HA monoclonal antibody and protein A-conjugated beads. After running the samples on SDS-PAGE, the gels were probed with streptavidin-horseradish peroxidase, which only reveals HA that was on the cell surface during biotinylation. The results presented in Fig. 3B show that all mutants were cleaved by trypsin into HA1 and HA2 as expected. In conclusion, the different fusion phenotypes of E11A and W14A are not the result of reduced expression per cell or cleavage by trypsin on the surface of the CV-1 cells, but the result of intrinsic differences of their fusion activities.

Binding of HA Fusion Peptide Mutants to Lipid Bilayers—To examine whether differences in the measured fusion activities could be caused by differences in binding or other modalities of lipid interaction of the different fusion peptide sequences to lipid model membranes, we prepared fusion peptides comprising the first 20 amino acids of the HA2

sequence followed by the highly polar and flexible sequence GCGKKKK. As described previously, this host-guest system greatly increases the solubility of these peptides and permits measurements of equilibrium binding to lipid bilayer model membranes from aqueous solution (20). The flexible linker between the guest and host portions of the peptide does not affect the fusion peptide-lipid interactions and the polar sequence substitutes for the polar ectodomain of HA as described previously.

We first measured the equilibrium partition coefficients for the binding of each of the peptides to lipid bilayers by isothermal titration calorimetry. The titration of SUVs to the F9A fusion peptide is shown in Fig. 4A as an example. After about eight injections all free peptide is bound to lipid, and the remaining spurious heats of reaction are the result of the enthalpies of dilution and mixing, which are corrected for by subtracting appropriate controls. From these data the fraction of bound peptide/mol of lipid, X_b , and the concentration of free peptide, C_f , are obtained. As shown in Fig. 4B, a plot of X_b versus C_f yields a straight line with a slope that is the apparent mol fraction partition coefficient, K_{app} . Such plots were obtained for each of the four mutant and the wild-type fusion peptides. The resulting partition coefficients are listed in Table 1. Most fusion peptides have K_{app} values in the range of 5.1 – $13.3 \times 10^5 \text{ M}^{-1}$, but W14A has a 10-fold lower K_{app} of $5 \times 10^4 \text{ M}^{-1}$.

All peptides except E11A have a net positive charge of 1, and E11A has a net positive charge of 2. Therefore, all peptides will be electrostatically attracted to the negatively charged membrane surfaces, and the peptide concentrations near the membrane will be higher than the bulk concentrations in solution. The electrostatic contribution to this interaction was calculated by the Gouy-Chapman theory and subtracted from the apparent partition coefficient to obtain the intrinsic mol fraction partition coefficient and corresponding free energy change (11, 20). As shown in Table 1, the free energy changes of the wild-type, F9A, E11A, and N12A fusion peptides are around -7 kcal/mol , but the $\Delta\Delta G$ of binding W14A is only -5.6 kcal/mol . The values of the former peptides are very similar to those reported previously for the wild-type peptide (10, 20). The good agreement of the binding constants and $\Delta\Delta G$ values confirms that these parameters can be measured reliably by a fluorescence method (10) or isothermal titration calorimetry (this work).

The enthalpy changes that are associated with the binding of fusion peptides to lipid bilayers were determined by a reverse titration isothermal titration calorimetry experiment (10). The integrated heats from each injection are measures of the reaction enthalpy as shown in Fig. 4, C and D. After subtraction of the appropriate controls, one obtains the enthalpy changes, $\Delta\Delta H$, of the binding of the mutant and wild-type fusion peptides to lipid bilayers, which are summarized in Table 1. The wild-type and the F9A and N12A mutants exhibit similar enthalpy changes of binding (about -15 to -16 kcal/mol), whereas E11A and W14A exhibit significantly smaller values of $\Delta\Delta H$, *i.e.* -10 and -9 kcal/mol , respectively.

The enthalpy changes (and to a lesser extent also the free energy and entropy changes, not shown) of the different peptides correlate quite well with the fusion activities of the corresponding mutants (Fig. 5). To extend the correlation to earlier results, the fusion activities and enthalpy changes of G1S and G1V are also included in this comparison. The nonfusion mutants G1V and W14A clearly show the lowest $\Delta\Delta H$ of binding. The hemifusion mutants G1S and E11A show intermediate values of $\Delta\Delta H$, and the wild-type and unimpaired mutants show the largest (negative) values of $\Delta\Delta H$.

Perturbation of Lipid Bilayer Order by HA Fusion Peptide Mutants—The perturbation of the lipid bilayer structure by the HA fusion peptide

TABLE 2

ATR dichroic ratios of the lipid methylene stretching vibrations and derived acyl chain order parameters in the absence and presence of bound fusion peptides

Results are the averages from three independent experiments each. WT, wild-type.

	R^{ATR}		S_L
	2920 cm^{-1}	2850 cm^{-1}	
Lipid only	1.36 ± 0.03	1.34 ± 0.03	0.34 ± 0.01
WT	1.16 ± 0.06	1.12 ± 0.05	0.58 ± 0.02
F9A	1.18 ± 0.04	1.17 ± 0.03	0.55 ± 0.01
E11A	1.25 ± 0.06	1.23 ± 0.05	0.47 ± 0.01
N12A	1.17 ± 0.03	1.16 ± 0.03	0.57 ± 0.01
W14A	1.32 ± 0.05	1.32 ± 0.05	0.38 ± 0.01

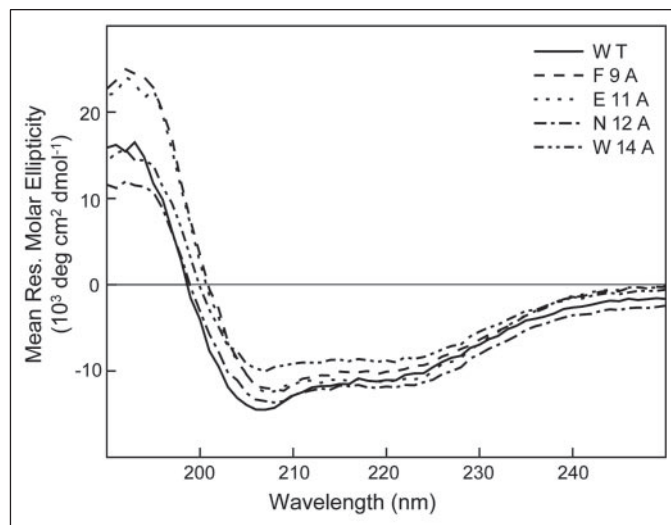


FIGURE 6. CD spectra of fusion peptides bound to lipid bilayers composed of POPC:POPG (4:1) at a peptide:lipid ratio of 1:100 and a peptide concentration of 0.1 mg/ml measured at pH 5 and 25 °C.

mutants was investigated by polarized ATR-FTIR spectroscopy. The order of the acyl chains in a fluid lipid bilayer is described by the order parameter S_L , which is an average of all angles θ from the membrane normal that are experienced by the methylene segments of the acyl chains.

$$S_L = \langle \cos^2\theta - 1 \rangle^{3/2} \quad (\text{Eq. 5})$$

S_L values for the bilayer in the presence and absence of the fusion peptides were determined from the ATR dichroic ratios, R^{ATR} , of the methylene stretching vibrations at 2920 cm^{-1} and 2850 cm^{-1} (Table 2). The theoretical range of these order parameters is from 0 to 1 for completely disordered to completely ordered acyl chains, respectively. The data of Table 2 indicate that the wild-type and the fusogenic mutant peptides F9A and N12A increase the order of the bilayer more than the fusion-deficient mutants W14A and E11A, as has been noted previously for other fusogenic and nonfusogenic HA fusion peptides (21, 22).

As noted above for the correlation of fusion of HA-expressing cells with the enthalpy of fusion peptide binding to model membranes, there is also a strong correlation between the fusion activity of HA-expressing cells and the increase of the order parameter of membrane lipids by the different fusion peptides (Fig. 5). This increase in order parameter most likely reflects the ability of the active fusion peptides to dehydrate the membrane surface, which is diminished in the case of the inactive fusion peptides (3, 21, 22).

Secondary Structures of HA Fusion Peptide Mutants in Lipid Bilayers—Circular dichroism (CD) spectra were recorded to assess the secondary structures of the mutant fusion peptides in lipid bilayers. Fig.

TABLE 3**Chemical shifts (ppm) and assignments of backbone and side chain protons of W14A fusion domain in DPC micelles at pH 5.0**

Residue	HN	H α	H β	Others
G1		3.938 4.014		
L2	9.392	4.102	1.70	γ CH2, 1.576; δ CH3, 0.857, 0.943
F3	8.982	4.235	3.209 3.154	2,6H, 7.275
G4	8.531	3.771 3.788		
A5	8.196	4.267	1.550	
I6	8.156	3.778	1.986	γ CH2, 1.898, 1.078; γ CH3, 0.947; δ CH3, 0.845
A7	8.537	3.923	1.373	
G8	8.202	3.919 3.879		
F9	7.909	4.449	3.303	2,6H, 7.256
I10	8.173	3.650	2.047	γ CH2, 1.281; γ CH3, 0.931; δ CH3, 0.886
E11	8.395	3.991	2.121	γ CH2, 2.477, 2.352
N12	8.084	4.655	2.813	δ NH $_2$, 7.660, 6.902
G13	8.178	3.784		
A14	8.424	3.933	1.379	
E15	8.233	4.032	2.108	γ CH2, 2.427, 2.347
G16	8.182	3.962		
M17	7.932	4.389	2.164 2.113	γ CH2, 2.570, 2.646
I18	7.849	4.145	1.920	γ CH2, 1.540, 1.174; γ CH3, 0.921; δ CH3, 0.861
D19	8.363	4.606	2.735	
G20	8.331	3.987		

6 shows that all peptides were partially helical (40–50%) when bound to POPC:POPG (4:1) bilayers. We also performed CD measurements at higher peptide:lipid ratios, such as those encountered at the beginning of the titration experiments of Fig. 4A. These spectra retained the typical minima at 208 and 222 nm, which are characteristic for helical secondary structure under all conditions (data not shown). Therefore, the peptides are unlikely to undergo major aggregation and conformational changes in the course of the binding experiments of Fig. 4.

Polarized ATR-FTIR spectra in the amide I' region were also consistent with partial α -helical structures of these peptides in lipid bilayers (data not shown). The measured dichroic ratio of the amide I' band of W14A was 1.48, which is consistent with the helical portion(s) of W14A inserted almost parallel to the membrane surface (12). The wild-type peptide had a dichroic ratio of 1.68 (20), which indicates a more oblique insertion of its helical portion into the lipid bilayer. The other peptides had intermediate dichroic ratios resulting in intermediate average insertion angles (data not shown).

Structure of the W14A Fusion Peptide—Because the W14A mutant had the most dramatic effect on the fusion activity of HA, we chose to determine by NMR the high resolution structure of this fusion peptide in micelles formed by the single chain lipid DPC. The CD spectrum of W14A in DPC micelles at pH 5 (not shown) is similar to that in lipid bilayers shown in Fig. 6. Therefore, DPC should be a good mimic of the bilayer environment, and structural features determined in DPC should be representative of those in lipid bilayers. TOCSY and NOESY spectra of W14A in DPC micelles in pH 5 buffer were recorded at 600 MHz. Sequential backbone and side chain resonance assignments were obtained for all residues and are listed in Table 3.

The chemical shifts of the amide (HN) and α -carbon (H α) protons are sensitive to the conformation of polypeptides (23). Fig. 7A shows HN and H α chemical shift differences of W14A from tabulated chemical shifts in random coils (23). In Fig. 7B, the HN and H α chemical shifts of W14A are compared with those of the wild-type fusion peptide (taken from Refs. 5 and 8) in DPC micelles at pH 5. According to these data, W14A is structured in DPC micelles. Except for Gly-8, the chem-

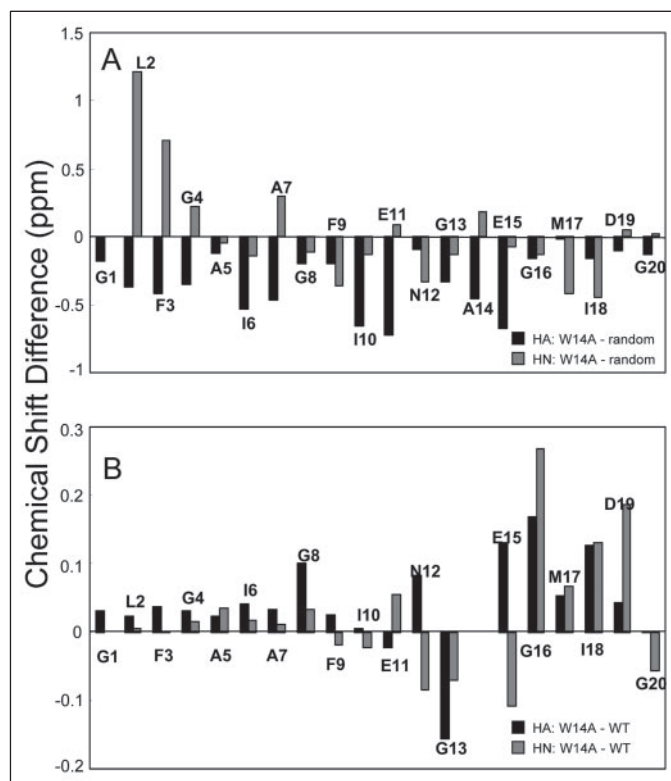


FIGURE 7. Backbone ^1H chemical shift differences (HN and H α) indicating structural differences between W14A and wild-type (WT) fusion peptides bound to DPC micelles at pH 5. A, differences $\delta_{\text{W14A}} - \delta_{\text{random coil}}$. B, differences $\delta_{\text{W14A}} - \delta_{\text{WT}}$.

ical shift differences are small for the first 11 residues but relatively large for residues 12–20. This indicates a significant difference in conformation of the C-terminal halves of the two structures.

The NOESY spectrum of W14A indicates the presence of all $d\alpha_{\text{N}}$ ($i, i+3$) and $d_{\alpha\beta}$ ($i, i+3$) and some $d\alpha_{\text{N}}$ ($i, i+4$) NOEs starting from residues $i = \text{Leu-2 to Gly-4}$ and $i = \text{Ile-6 to Phe-9}$. This confirms the presence of helical structures from Leu-2 to Ala-5 and Gly-8 to Glu-11 of the W14A peptide. However, there are no NOEs between H α (Ala-5) and H β (Gly-8) or HN(Gly-8) or Phe-9). Ala-5 also had nearly random HN and H α chemical shifts. This indicates a break in the N-terminal helix of the W14A fusion peptide structure at residues Ile-6 and Ala-7. In the wild-type peptide, NOEs between Q δ (Phe-9) and H ϵ 3(Trp-14) and between H α (Ile-10) and H ϵ 3(Trp-14) are found (5, 8). In addition, there are NOEs between H α (Phe-9) and HN(Asn-12) and between HN(Asn-12) and HN(Trp-14). These NOEs, which in addition to the chemical shift data all contribute to defining the kink in the wild-type structure, are absent in the W14A structure, indicating that important interactions in the hydrophobic pocket of the wild-type fusion peptide are missing in the W14A mutant fusion peptide.

200 structures were calculated from a total of 145 nonredundant upper limit distance constraints and 61 dihedral angle constraints obtained from the experimental NOEs and chemical shifts of the W14A peptide. The backbone structures of the 40 lowest energy conformers are shown in Fig. 8, and the structural statistics are summarized in Table 4. Three different views of a typical conformation of the W14A peptide with side chains are shown in Fig. 9. Although the structure superficially looks similar to the wild-type structure with a bend in the middle, it is actually very different and much more flexible than the wild-type structure as described in more detail below.

A salient feature of the structure families presented in Fig. 8 is that the segment from residue Asn-12 to Ala-14 of W14A is very flexible. The

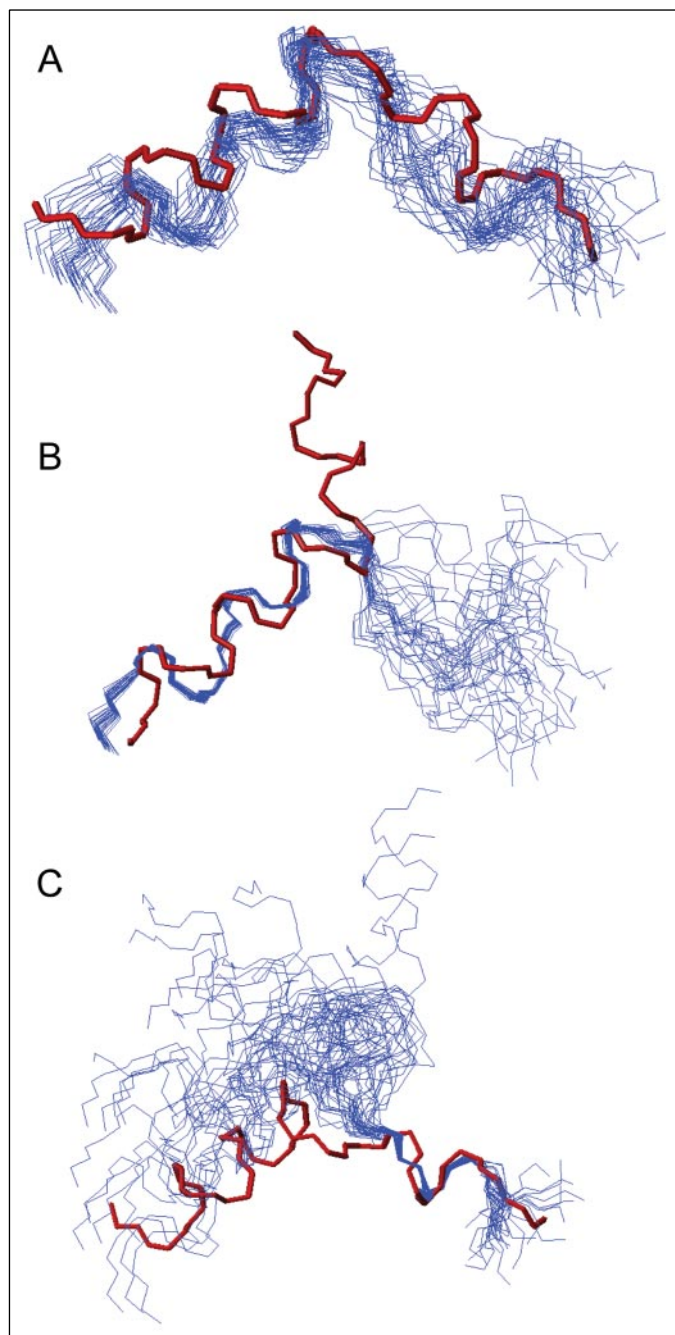


FIGURE 8. 40 lowest energy conformers of W14A fusion peptide in DPC micelles at pH 5. *A*, all residues (1–20) aligned. *B*, residues 2–12 aligned. *C*, residues 15–18 aligned. The red structures are those of the wild-type fusion peptide measured under identical condition and shown for comparison (from Ref. 5).

alignment of the 40 lowest energy conformers is poor when all 20 residues are aligned (Fig. 8*A*). Most conformers show a shallow V-shape structure, which is less compact than the wild-type structure. However, when residues 2–11 or 15–18 are aligned separately, the alignments between these structures are very good (Fig. 8, *B* and *C*). The root mean square displacements of the backbone atoms of the separately aligned segments are 0.30 ± 0.12 Å and 0.24 ± 0.14 Å, respectively, but the backbone root mean square deviation with the entire peptide aligned is high (2.16 ± 0.67 Å; Table 4). A closer inspection of Fig. 9 (and similar figures generated from other conformers) reveals that the two ordered arms of the flexible molecule are oriented in very different directions in all conformers of W14A than they are in the fixed angle structure of the

TABLE 4
Structural statistics of the NMR structures of the W14A fusion domain in DPC micelles at pH 5

Target function (Å)	0.090 ± 0.001
Experimental NMR constraints	
NOE distance constraints	145
Intraresidue	33
Sequential	66
Medium Range	46
Long Range	0
Angle constraints	61
Phi	25
Psi	17
Chi1	10
Chi2	9
NMR constraint violations	
NOE constraint violations	
Sum (Å)	2.04 ± 0.14
Maximum (Å)	0.10 ± 0.00
Angle constraint violations	
Sum (°)	4.11 ± 1.42
Maximum (°)	1.47 ± 0.39
AMBER energy (kcal/mol)	−204.3 ± 34.1
Root mean square deviation from mean structure (Å)	
Backbone atoms of all residues 1–20	2.16 ± 0.67
Heavy atoms of all residues 1–20	2.82 ± 0.78
Backbone atoms of residues 2–12	0.30 ± 0.12
Heavy atoms of residues 2–12	0.88 ± 0.29
Backbone atoms of residues 15–18	0.24 ± 0.14
Heavy atoms of residues 15–18	1.16 ± 0.31
Ramachandran statistics analyzed using PROCHECK-NMR	
Residues in allowed regions	100%

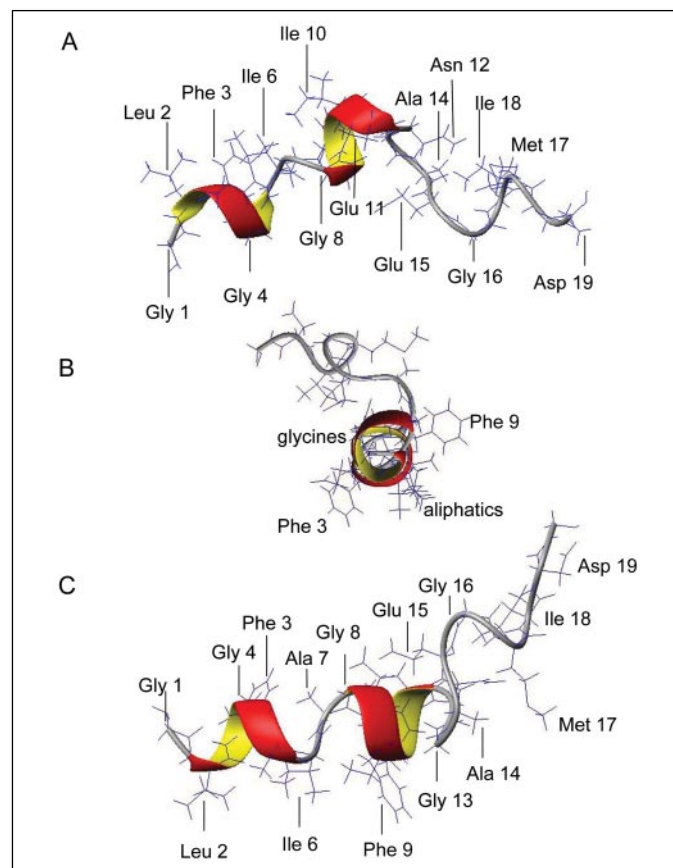


FIGURE 9. Three different views (orientations) of a typical structure of W14A fusion peptide in DPC micelles at pH 5.

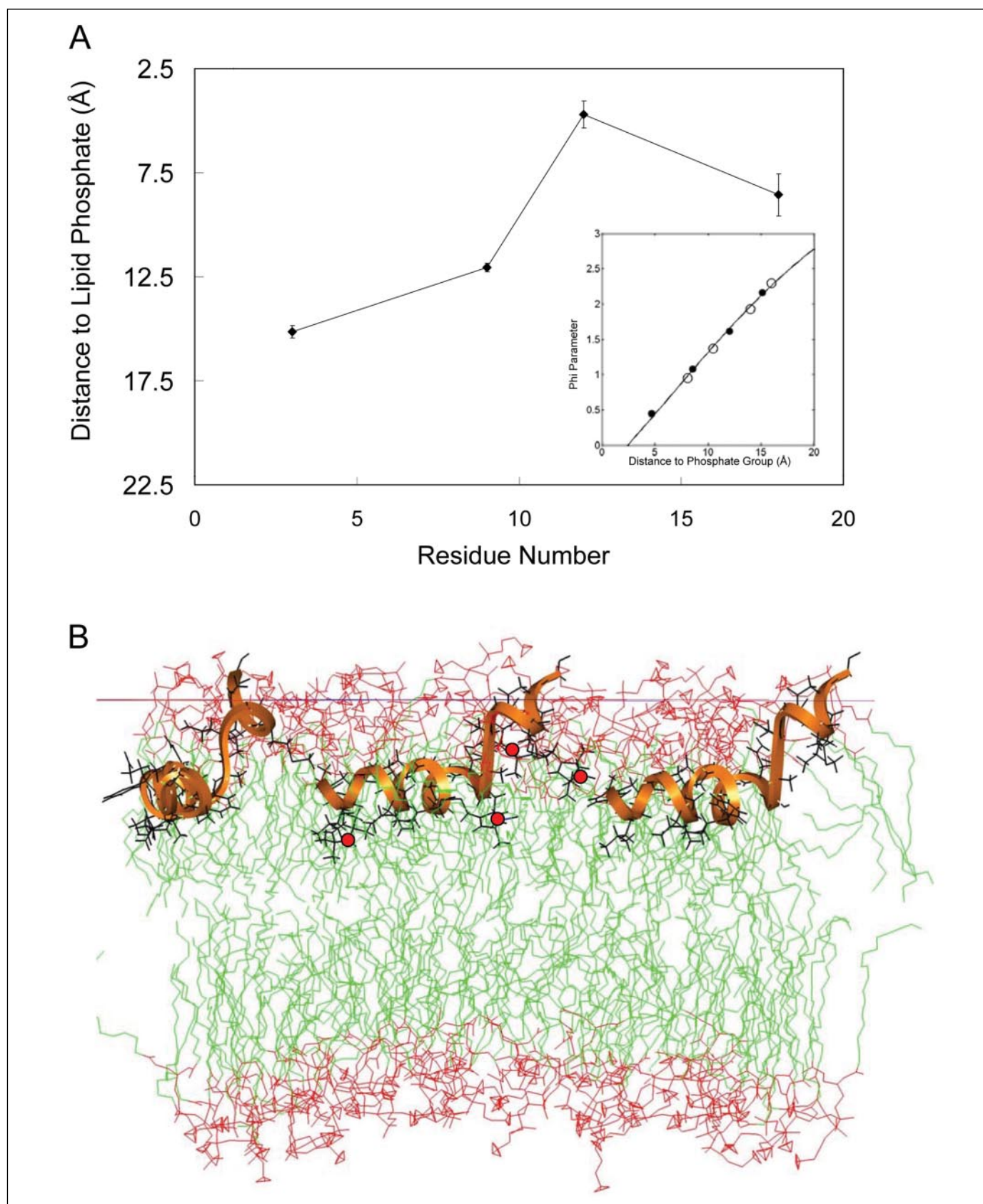


FIGURE 10. *A*, depth of four side chains (Phe-3, Phe-9, Glu-11, and Ile-18) of the W14A fusion peptide in lipid bilayers as determined by site-directed spin labeling and power saturation EPR spectroscopy. The *inset* shows the best fit calculated distances from NMR structures (*abscissa*) to experimental depths parameters (*ordinate*) of W14A and distances of spin-labeled lipids used in the same bilayers for calibration. *B*, W14A structure docked to a POPC lipid bilayer using the EPR distance constraints of *A*. The structure in the *middle* has all four spin labels grafted onto the NMR conformer shown in Fig. 9. The native W14A structure is shown in the same orientation to the *right* and an end-on view to the *left*. The *thin red line* represents the average position of the lipid phosphates.

wild-type fusion peptide. Another interesting difference between the W14A and wild-type structures is that the N-terminal arm of the W14A structure features a broken two-segment helix. Residues 2–5 actually form a 3_{10} -helix, and residues 8–11 form an α -helix with residues 6 and 7 not participating in any regular secondary structure. These residues form a bend of $\sim 135^\circ$ in this region, which is fixed in all calculated structures (Fig. 8B). Finally, residues 15–18 do not form the C-terminal single-turn helix in W14A as they do in the pH 5 wild-type structure. Instead, these residues form a rather irregular secondary structure that vaguely resembles those found in the pH 7 wild-type structure (5) or the pH 5 G1V mutant structure (8).

Placement of the W14A Fusion Peptide in Lipid Bilayers—To gain information about how the W14A fusion peptide is inserted into lipid bilayers, we determined the depth of penetration of four residues in the bilayer by site-directed spin labeling and power saturation EPR measurements in the presence of O_2 , N_2 , and NiEDDA (24). This method has been shown previously to determine the placement of the wild-type fusion domain in lipid bilayers with an accuracy of about $\pm 2 \text{ \AA}$ (5, 8). The bilayer penetration depths of residues 3, 9, 11, and 18 of the W14A fusion peptide are shown in Fig. 10A.⁵ Phe-3 and Phe-9 penetrate quite deeply into the bilayer, whereas the locations of Glu-11 and Ile-18 are shallower. Although we know that the W14A structure is quite flexible, we docked a selected typical NMR structure to the EPR distance constraints in bilayers. Three views of the docked structure are shown in Fig. 10B. The N-terminal helical arm of the peptide is inserted just below the polar head group region almost parallel to the plane of the membrane. The two segments of the N-terminal helix of the W14A fusion peptide lie flat in the interface stabilized by Phe-3 and Phe-9, which flank an aliphatic central section that dips most deeply into the hydrophobic core of the lipid bilayer (see also Fig. 9B). This orientation is consistent with the polarized ATR-FTIR data described above, which also showed a parallel orientation of the helical portions of the peptide in the bilayer. Clearly, both arms of the W14A structure take very different orientations in membranes than the two arms of the wild-type boomerang structure (compare Fig. 10B with Fig. 6 in Ref. 5). We realize that the model shown in Fig. 10B refers to only one conformer of a highly flexible molecule. However, none of the conformers of W14A inserts into the bilayer as a downward oriented boomerang as does the wild-type structure. Rather to the contrary, all docked conformers of the W14A fusion peptide have their C-terminal arms oriented at various angles upward and out of the membrane.

CONCLUSIONS

Our aim was to investigate the importance of the kink region of the HA fusion peptide to confer membrane fusion function. We hypothesized that a kinked boomerang structure with a conserved hydrophobic pocket and stabilizing hydrogen bonds is essential for the fusion activity of HA. Indeed, the fusion-defective mutant W14A has a fusion peptide structure in membranes which is very different from the fixed angle boomerang structure of the wild-type. The kink in the wild-type structure is stabilized by backbone hydrogen bonds between residues 11 and 8, 12 and 9, and 14 and 9, and a side chain hydrogen bond from Asn-12 to Ile-8 (5, 8). These bonds are all absent in W14A. Replacing the bulky

⁵ In previous work (5), we have proven more rigorously, *i.e.* with 18 EPR data points, that the wild-type structures at pH 5 and 7.4 are similar in DPC micelles and lipid bilayers. For all peptides of this work, we also observed very similar CD spectra in the two media. Unfortunately, it is unpractical and very costly to make 18 individual Cys mutants of each mutant by chemical synthesis. However, by extrapolation from wild-type data, we assume that the matches of the mutant structures in the two environments are of similar high quality as the matches of the wild-type structures in the two environments.

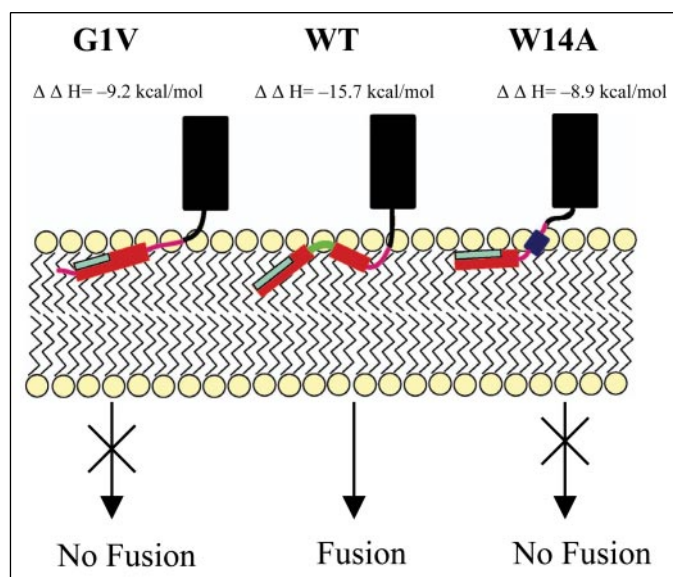


FIGURE 11. Schematic representation of the structures of the wild-type (WT) and two fusion-defective mutant HA fusion peptides in a lipid bilayer. The helical portions are shown in red and the disordered regions in pink. The fixed angle kink in wild-type is shown in green, the flexible kink in W14A in pink, and the ordered C-terminal secondary structure of W14A in dark blue. The light blue boxes represent the positions of the glycines in the N-terminal helices. The black parts represent portions of the ectodomain of HA. The enthalpies of fusion peptide binding to lipid bilayers are as indicated.

Trp-14 with a small Ala abolishes the ability to form a stable hydrophobic pocket in the inner angle of the kink and therefore opens this structure. Another fusion-defective mutant, G1V, adopts an irregular linear helical structure in membranes (8). Contrary to that structure, W14A is still kinked, but the kink is (a) flexible and (b) points in very different directions than in the wild-type structure (Fig. 11). Therefore, there are at least two different modes of breaking the boomerang and disrupting the fusion activity of HA fusion peptides: either by abolishing the kink altogether as observed in G1V or by making a flexible hinge that presumably cannot transduce force into the bilayer as observed in W14A.

The differences between the binding enthalpies of the active and inactive fusion peptides are quite instructive. The limited data that are currently available suggest that peptides that insert at a steeper angle (and have the ability to support membrane fusion in the context of the whole protein) have stronger interaction energies with lipid bilayers than the nonfusogenic peptides G1V and W14A, which lie shallower in the membrane interface. Perhaps the angled and more vertically inserted fusion peptides pack better with the hydrocarbon chains of the lipids than horizontally inserted peptides. This mode of lipid insertion may also be more conducive for the fusion peptide to interact with and perhaps slide down along the transmembrane domain of the fusion protein as proposed in the spring-loaded boomerang model of membrane fusion (6).

The larger binding enthalpies of the active fusion peptides are accompanied by smaller entropic contributions to their binding. We think that the greater entropy losses upon binding of active fusion peptides are the result of an ordering of lipids which is observed with the active fusion peptides but not with the inactive fusion peptides (Table 2). The reason for this effect may again be the better “fit” of the active fusion peptides with the lipid bilayer structure. As we have shown before, an ordering of the lipid chains could be accompanied by a partial dehydration of the membrane surface as a prelude to fusion.

Our initial hypothesis was that the hydrogen bonds within the kink region help to stabilize the boomerang shape. However, our results confirm this hypothesis only partially. The replacement of Asn-12 with an

Influenza Fusion Peptide Kink Mutations

Ala does not affect the activity of the fusion peptide. Apparently, the side chain hydrogen bond of Asn-12 is not required to maintain an active structure. Although Trp-14 proved to be important for forming the hydrophobic pocket, Phe-9 apparently is not as critical, although it lines the other side of the pocket at a similar depth in the membrane (5). Ala in this position is perhaps not disruptive enough, and the bulky hydrophobic side chain of Ile-10 may partially substitute for Phe-9. An interesting open question is why E11A causes hemifusion. The structure of another hemifusion mutant HA fusion peptide, G1S, has been solved and found only to disrupt the glycine edge on the N-terminal arm on the boomerang. Glu-11 is located at the other end of this arm of the boomerang in direct continuation of the glycine edge. The susceptibility of this location to transforming an active into a partially active fusion peptide again suggests that this face of the N-terminal helix is very important for driving fusion from the hemifusion to the full fusion stage. Further studies of E11A, especially determining the structure of its fusion peptide, may provide interesting new clues about this last step in membrane fusion.

Acknowledgments—We thank Dr. D. Cafiso for the use of his EPR spectrometer.

REFERENCES

1. Skehel, J. J., and Wiley, D. C. (2000) *Annu. Rev. Biochem.* **69**, 531–569
2. Earp, L. J., Delos, S. E., Park, H. E., and White, J. M. (2005) *Curr. Top. Microbiol. Immunol.* **285**, 25–66
3. Lai, A. L., Li, Y., and Tamm, L. K. (2005) in *Protein-Lipid Interactions* (Tamm, L. K., ed) pp. 279–303, Wiley-VCH, Weinheim, Germany
4. Chen, J., Skehel, J. J., and Wiley, D. C. (1999) *Proc. Natl. Acad. Sci. U. S. A.* **96**, 8967–8972
5. Han, X., Bushweller, J. H., Cafiso, D. S., and Tamm, L. K. (2001) *Nat. Struct. Biol.* **8**, 715–720
6. Tamm, L. K. (2003) *Biochim. Biophys. Acta* **1614**, 14–23
7. Qiao, H., Armstrong, R. T., Melikyan, G. B., Cohen, F. S., and White, J. M. (1999) *Mol. Biol. Cell* **10**, 2759–2769
8. Li, Y., Han, X., Lai, A. L., Bushweller, J. H., Cafiso, D. S., and Tamm, L. K. (2005) *J. Virol.* **79**, 12065–12076
9. Armstrong, R. T., Kushnir, A. S., and White, J. M. (2000) *J. Cell Biol.* **151**, 425–437
10. Li, Y., Han, X., and Tamm, L. K. (2003) *Biochemistry* **42**, 7245–7251
11. Han, X., and Tamm, L. K. (2000) *J. Mol. Biol.* **304**, 953–965
12. Tamm, L. K., and Tatulian, S. A. (1997) *Q. Rev. Biophys.* **30**, 365–429
13. Luginbühl, P., Güntert, P., Billeter, M., and Wüthrich, K. (1996) *J. Biomol. NMR* **8**, 136–146
14. Koradi, R., Billeter, M., and Wüthrich, K. (1996) *J. Mol. Graph* **14**, 51–55, 29–32
15. Langen, R., Oh, K. J., Cascio, D., and Hubbell, W. L. (2000) *Biochemistry* **39**, 8396–8405
16. Zaitseva, E., Mittal, A., Griffin, D. E., and Chernomordik, L. V. (2005) *J. Cell Biol.* **169**, 167–177
17. Gething, M. J., Doms, R. W., York, D., and White, J. (1986) *J. Cell Biol.* **102**, 11–23
18. Schoch, C., and Blumenthal, R. (1993) *J. Biol. Chem.* **268**, 9267–9274
19. Steinhauer, D. A., Wharton, S. A., Skehel, J. J., and Wiley, D. C. (1995) *J. Virol.* **69**, 6643–6651
20. Han, X., and Tamm, L. K. (2000) *Proc. Natl. Acad. Sci. U. S. A.* **97**, 13097–13102
21. Gray, C., Tatulian, S. A., Wharton, S. A., and Tamm, L. K. (1996) *Biophys. J.* **70**, 2275–2286
22. Han, X., Steinhauer, D. A., Wharton, S. A., and Tamm, L. K. (1999) *Biochemistry* **38**, 15052–15059
23. Wishart, D. S., Sykes, B. D., and Richards, F. M. (1992) *Biochemistry* **31**, 1647–1651
24. Altenbach, C., Greenhalgh, D. A., Khorana, H. G., and Hubbell, W. L. (1994) *Proc. Natl. Acad. Sci. U. S. A.* **91**, 1667–1671